JP2.17 Refractivity Data Assimilation

Qin Xu*, National Severe Storms Laboratory, Norman OK
Kang Nai, CIMMS, University of Oklahoma, Norman OK
Ted Rogers, Space and Naval Warfare Center, San Diago, California
Tracy Haack and Stephen Burk, Naval Research Laboratory, Monterey CA

1. Introduction

Low-altitude nearly-horizontal electromagnetic (EM) propagation is strongly affected by the presence of surface-based and elevated ducts. These ducts can be formed by capping inversions in the marine atmospheric boundary layer in subsidence-driven regimes such as that experienced in the southern California bight. Such ducts are also formed by thermal internal boundary layers that can exist when warm continental air flows over a cooler ocean, a regime that is common on the east coast of the United States. There exist many ways of estimating the duct structures or some of their aspects: in situ methods (radiosondes and rocketsondes), using mesoscale models, and by remote sensing, including inference of refractivity parameters from GPS signals and from radar sea clutter. However, no method exists to tie the information from these different sources in near-real-time. The objective of refractivity data assimilation is to develop that capability.

Modified refractivity is a convention used within the EM propagation community which can be calculated as a function of height (above the ground or sea surface) by

$$M(z) = 77.6(p + 4810\, e/T)/T + 0.157z,$$

where p is the pressure (mb), e the water vapor pressure (mb), T the temperature (K), and z the height (m). The advantage of using M is that upward/downward refracting regions are identified by positive/negative refractivity gradients (dM/dz). In the presence of an inversion, the refractivity profile is often characterized as being tri-linear determined by three key variables: the base height h, the intensity ΔM, and the thickness Δz of the inversion. Here, h and ΔM, have respectively strong negative and positive correlations with signal strengths, an expected behavior as they, from a ray perspective, determine the critical angle for trapping energy within a duct. From a ray perspective, Δz has no influence on the degree of trapping. More rigorous modeling using a parabolic equation (PE) or wave-guide model shows that it does – however, we might consider it a second-order effect in comparison with h and ΔM. We suspect that these variables -- or some variation or augmentation of the same -- can also account for refractivity profiles associated with thermal internal boundary layers. However, that has not yet been demonstrated.

* *Corresponding author address:* Qin Xu, NSSL/NOAA, 1313 Halley Circle, Norman, OK 73069; e-mail: Qin.Xu@nssl.noaa.gov.

Clearly, h, ΔM, and Δz are nonlinear functions of the primitive variables (pressure, temperature and humidity) and they are not directly analyzed by the conventional optimal interpolation or 3-dimensional variational method (3dVAR). As a linear interpolator, the conventional 3dVAR cannot correct phase errors in $M(z)$. Instead, it may produce spurious double inversion layers when the observed inversion layer is entirely above or below the background inversion layer (provided by the model forecast). The vertical correlation functions used in the conventional 3dVAR are often too smooth and thus smear the inversion. The inversion-related problems are notorious in boundary layer data assimilation. We assume those errors are costly in the refractivity data assimilation problem considered here.

The inversion-related vertical phase error problems may be eliminated if the vertical phase error in the background inversion can be corrected by stretching the vertical coordinate along each grid column. The latter, however, requires the two-dimensional field of the inversion base height h be correctly estimated. To this end, an automated algorithm is developed to detect inversion layers and compute duct parameters from radiosonde observations and model forecasts (the details are omitted) and then a 2dVAR is developed to "optimally interpolate" the duct parameters from observation locations to the model grid. The error statistics required by the 2dVAR are estimated from the innovations (observations minus forecasts) obtained from the Variability of Coastal Atmospheric Refractivity (VOCAR) field experiment (Fig. 1).

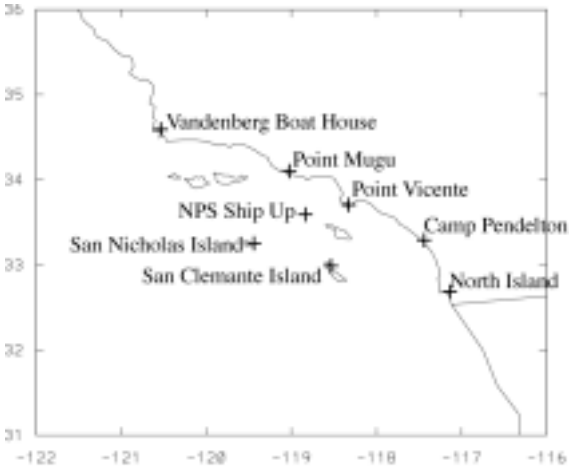

Fig. 1. VOCAR radiosonde stations used for innovation analysis for the period from 8/23/93 to 9/04/93. The innovations are given by the VOCAR observations (every 4 hours) minus the forecasts (of 4, 8, 12 hours) from the Navy Operational Regional Atmospheric Prediction System (NORAPS with 20 km horizontal resolution and 30 vertical levels, see Burk and Thompson, 1997; Rogers et al. 1996)

2. Basic assumptions and error statistics

The base height innovation at the i-th observation station is defined by $h^{d}_{i} + h^{o}_{i} - h^{f}_{i} = h''_{i} - h'_{i}$, where $(\bullet)^{o}$ denotes the observation, $(\bullet)^{f}$ the forecast, $(\bullet)''$ the observation error, and $(\bullet)'$ the forecast error. All the observations are assumed to be unbiased but have random errors that are not correlated between different stations and independent of forecast errors. Thus, the forecast bias is given by the innovation bias:

$$<h'_{i}> = -<h^{d}_{i}>, \qquad (1)$$

where $<(\bullet)>$ the ensemble mean or time mean (under the ergodicity assumption). The unbiased part of the forecast error is horizontally correlated. The auto-correlation function is assumed to be Gaussian-elliptical and is denoted by $R_{hh}(\mathbf{r}_{ij}, a, b, ß)$ where $\mathbf{r}_{ij} = \mathbf{x}_i - \mathbf{x}_j$ is the horizontal vector distance between the two correlation points i and j, $\mathbf{x} + (x, y)$, a and b are the correlation length scales along the long and short axes of the ellipse, respectively, and ß is the angle between the x-coordinate and the long axis of the ellipse.

The normalized innovation is defined by $H^{d}_{i} + [h^{d}_{i} - <h^{d}_{i}>]/\sigma_h^{d}(\mathbf{x}_i)$ where

$$\sigma_h^{d}(\mathbf{x}_i)^2 = <(h^{d}_{i} - <h^{d}_{i}>)^2> \qquad (2)$$

is the innovation variance. Based on the above assumptions, the covariance of H^{d}_{i} can be partitioned as follows:

$$<H^{d}_{i}H^{d}_{j}> = [1 - c(\mathbf{x}_i)c(\mathbf{x}_j)]\delta_{ij} + c(\mathbf{x}_i)c(\mathbf{x}_j)R_{hh}(\mathbf{r}_{ij}, a, b, ß). \qquad (3)$$

where $c(\mathbf{x}_i) = \sigma_h^{f}(\mathbf{x}_i)/\sigma_h^{d}(\mathbf{x}_i)$, and $\sigma_h^{f}(\mathbf{x}_i) = <(h'_{i} - <h'_{i}>)^2>^{1/2}$ is the forecast error standard deviation. Note that $<H^{d}_{i}H^{d}_{i}> = 1$, $\delta_{ii} = 1$, $\mathbf{r}_{ii} = 0$, $R_{hh}(\mathbf{r}_{ii}, a, b, ß) = 1$, so when i = j the two terms on the righthand side of (3) represent, respectively, the observation and forecast error variances normalized by the innovation variance. To reduce the number of unknowns, $c(\mathbf{x}_i)$ is assumed to be constant and this treatment is similar to the innovation analyses of Hollingsworth and Lönnberg (1986) and Xu et al (2001). The four parameters (a, b, ß, c) are determined by least-square fitting of the analytical expression on the righthand side of (3) to the values of $<H^{d}_{i}H^{d}_{j}>$ computed from the VOCAR innovation data. The results are listed in Table 1. By setting $a = b$ and ß = 0, the correlation function reduces to Gaussian-isotropic (see Fig. 2).

The above innovation method is similarly used to estimate the error variances and auto-correlation functions for the remaining two duct parameters. The resulting parameter values for the ΔM-ΔM auto-correlation are listed in the second row of Table 1. The Δz-Δz auto-correlation, however, is found to drop rapidly to nearly zero as $|\mathbf{r}_{ij}|$ increases to about 70 km and then fluctuate around zero as $|\mathbf{r}_{ij}|$ increases beyond 70 km. Since the horizontal correlation length scale for the Δz-Δz auto-correlation error is only about 50 km and is shorter than the spacing between most of the VOCAR stations, the 2dVAR analysis of Δz becomes ineffective. For the time being, we avoid the 2dVAR analysis of Δz. We note, however, that the vertical profile of refractivity within the interfacial layer, in particular the presence of a "sharp top" can have a significant affect on EM propagation. At the same time, the ability to realistically estimate the profile of refractivity within the interfacial layer within the framework of the mesoscale model is somewhat limited at present. So we might expect to return to the analysis of Δz at some point in the future. All the cross-correlations (h-ΔM, h-Δz and ΔM-Δz) are found to be insignificant for the VOCAR data, so only an univariate version of 2dVAR is considered in section 4.

Table 1. Parameter values

	a (km)	b(km)	ß (^{o})	c
for h	400	290	56.0	0.66
ΔM	220	173	37.1	0.64

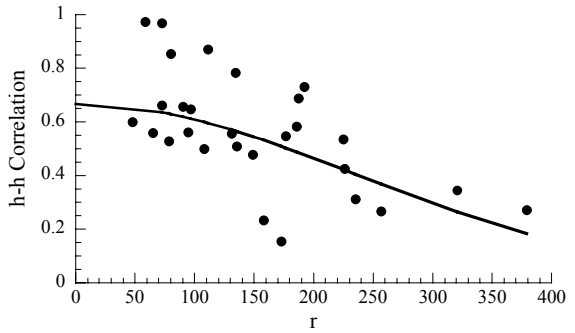

Fig. 2. Least-square fitting of isotropic h-h auto-correlation function (solid curve) to innovation correlation data (dots). The resulting parameter values are $a = b = 333.5$ km and $c = 0.6663$.

3. Forecast bias and error standard deviation

After the forecast bias is computed from (1) at each station, the bias field $b_h(\mathbf{x})$ is modeled by thin-plate spline by minimizing the following costfunction

$$J = \sum(b_h(\mathbf{x}_i) - \langle h'_i \rangle)^2 + \mu \|\Delta_H b_h(\mathbf{x})\|, \qquad (4)$$

where Δ_H is the horizontal Laplacian, μ is the weight for the thin-plate penalty term (see Chapter 2 of Wahba 1990). If the bias computed from (1) at each station is sufficiently accurate, then $\mu \varnothing 0$ and the minimizer of (4) is given by the solution of the following boundary value problem:

$$\Delta_H^2 b_h = 0 \quad \text{for } \mathbf{x} \neq \mathbf{x}_i$$
$$b_h = \langle h'_i \rangle \text{ and } {}_H b = 0 \text{ at } \mathbf{x} = \mathbf{x}_i,$$
$$b(\mathbf{x}) \varnothing \Sigma \langle h'_i \rangle / N \quad \text{for } |\mathbf{x}| \varnothing \quad ,$$

where ${}_H$ denotes the horizontal gradient and Σ the summation from 1 to N (the total number of observation sets). The estimated bias field is plotted in Fig. 3a.

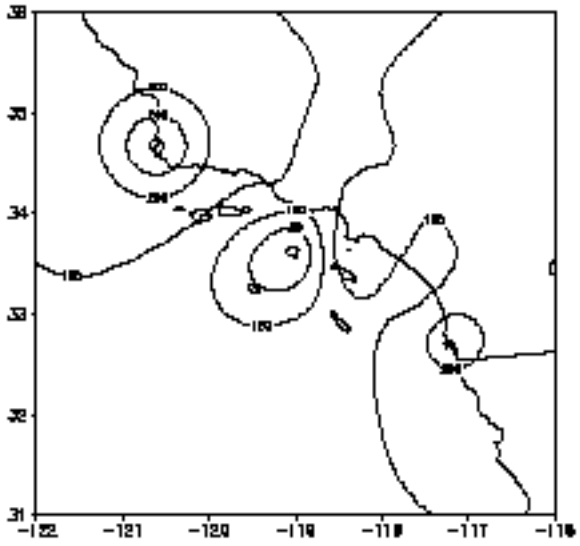

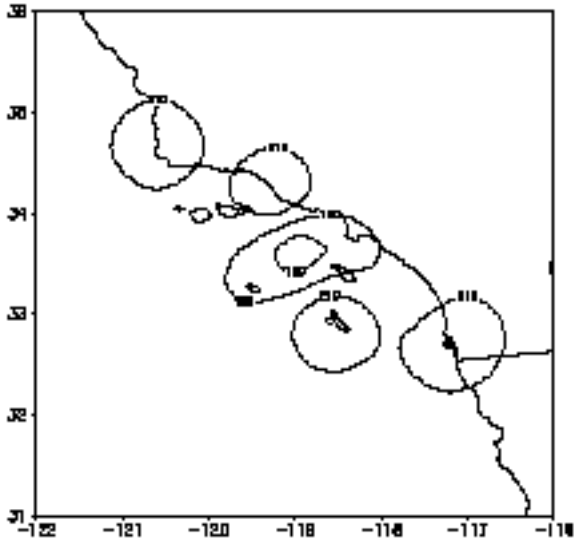

Fig. 3. Base height forecast bias (a) and forecast error standard deviation (b).

The above thin-plate spline model is also used to estimate the forecast error standard deviation field $\sigma_h^f(\mathbf{x})$ and the result is plotted in Fig. 3b. The bias field and error standard deviation field for ΔM forecast are modeled similarly and the details are omitted.

4. 2dVAR analysis

The 2dVAR analysis leads to the following vector equation for the analysis of the inversion base height:

$$\mathbf{h}^a = (\mathbf{h}^f - \mathbf{b}) + \mathbf{F}\mathbf{H}^T\mathbf{Q}^{-1}[\mathbf{h}^o - \mathbf{H}(\mathbf{h}^f - \mathbf{b})],$$

where $\mathbf{h}^f$ and $\mathbf{b}$ are the forecast and forecast bias (vectors in the model grid space), respectively, $\mathbf{h}^o$ the observation (vector in the observation space), $\mathbf{H}$ the observation operator (transformation matrix from the model grid space to observation space), and $\mathbf{Q} = \mathbf{H}\mathbf{F}\mathbf{H}^T + \mathbf{O}$. $\mathbf{F}$ and $\mathbf{O}$ are the forecast and observation error covariance matrices, respectively, and they are computed from the error variances and correlation obtained in sections 2 and 3.

Although the VOCAR data are limited to 8 stations (Fig. 1), the 2dVAR works well as shown by the comparison between the forecast and analyzed base height fields in Figs. 4a-b. The analyses are compared with the forecasts and observations of h for the entire VOCAR period at the San Clemente Island (Fig. 5a) and Point Mugu (Fig. 5b). As shown, the 2dVAR is effective in correcting the forecast bias and filtering random observation errors, and this effectiveness is seen not only in space but also in time although the analysis is performed in space only). Similar

effectiveness is seen for the analyses of ΔM in Figs. 6a-b.

Radio propagation measurements can be related nonlinearly, with some degree of ambiguity, to the duct parameters (Rogers 1997). These measurements can be assimilated together with the radiosonde observations by upgrading the current 2dVAR. This problem is under investigation.

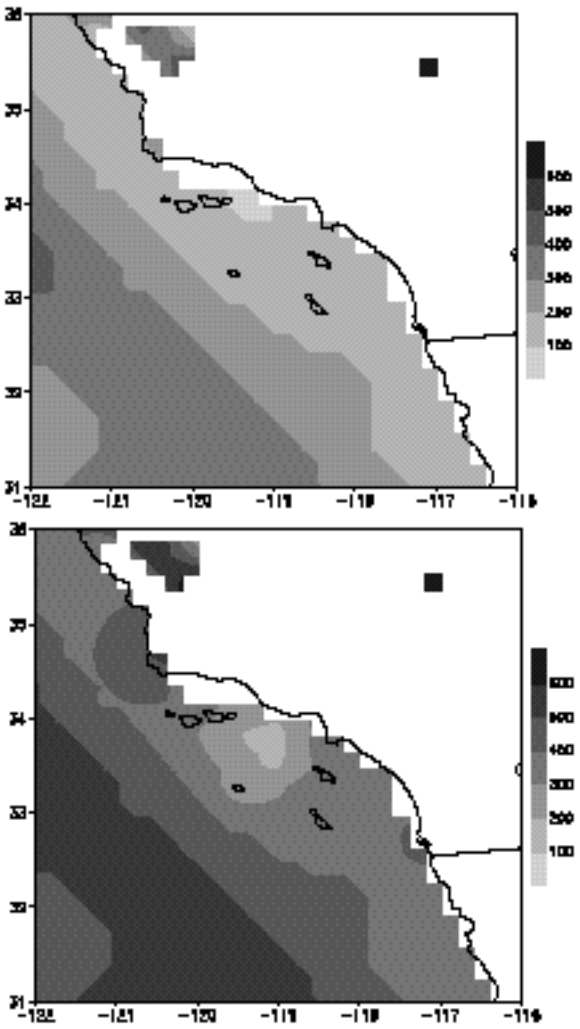

Fig. 4. Base height (in m) at 20:00 UTC 9/2/1993 from NORAPS forecast (a) and 2dVAR analysis (b).

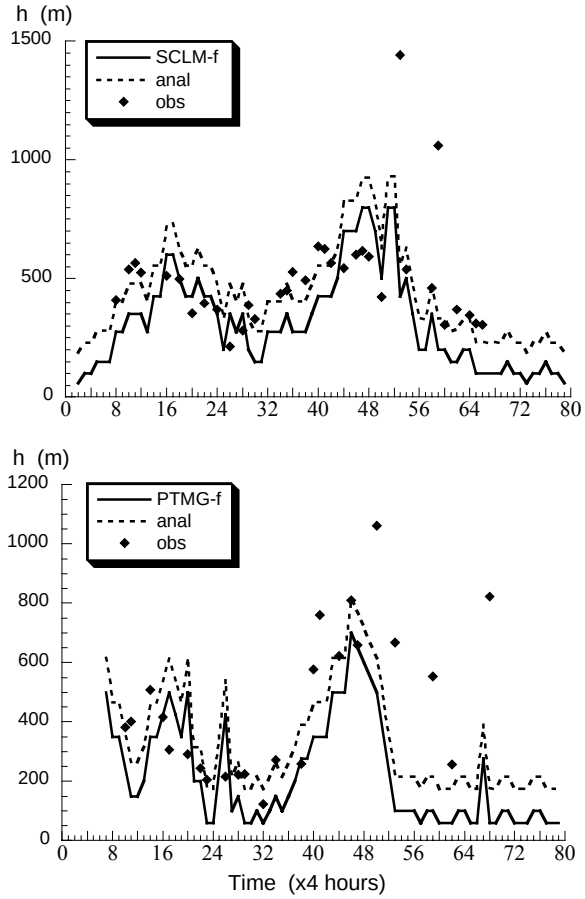

Fig. 5. Time series of forecast, observation and analysis of *h* at (a) San Clemente Island and (b) Point Mugu.

Acknowledgments: The research work was supported by the Office of Naval Research through FD-SDSU contract N66001-97-D-5028 to the University of Oklahoma.

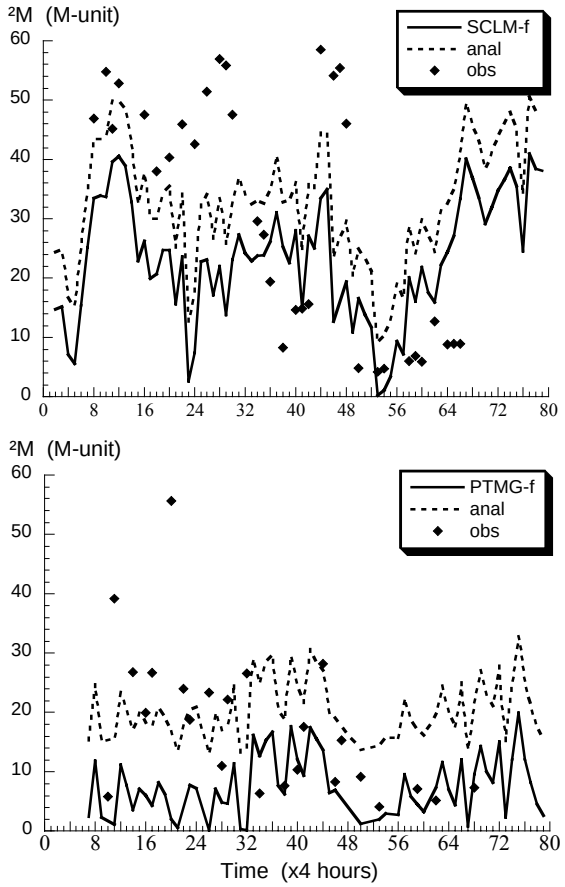

Fig. 6. As in Fig. 5 but for time series of ΔM.

References

Burk, S.D. and W.T. Thompson, 1997: Mesoscale modeling of summertime refractive conditions in the Southern California bight. *J. Appl. Meteor.*, **36**, 22-31.

Hollingsworth, A., and P. Lönnberg, 1986: The statistical structure of short-range forecast errors as determined from radiosonde data. Pat I: The wind field. *Tellus*, **38A**, 111-136.

Rogers, L. T., 1997: Likelihood Estimation of tropospheric duct parameters from horizontal propagation measurements. *Radio Science*, **32**, 79-92.

Rogers, L. T., R. A. Paulus, and J. Cook, 1996: Fusing data from the mesoscale model and radio remote sensing. *Proc. Battlespace Atmospherics Conference*, San Deigo, CA, (3-5 Dec. 1996), NRaD Tech. Doc. 2938, pp. 283-291.

Wahba, G, 1990: *Spline models for observational data*. Captial City Press, Montpelier, Vermont, 169 pp.

Xu, Q., L. Wei, A. VanTuyl and E. H. Barker, 2001: Estimation of three-dimensional error covariances. Part I: Analysis of height innovation vectors. *Mon. Wea. Rev*. (in press).